THE JOURNAL OF BIOLOGICAL CHEMISTRY Vol. 280, No. 34, Issue of August 26, pp. 30460–30468, 2005

Printed in U.S.A.

β2 Subunit Contribution to 4/7 α-Conotoxin Binding to the Nicotinic Acetylcholine Receptor*

Received for publication, April 19, 2005, and in revised form, June 1, 2005
Published, JBC Papers in Press, June 1, 2005, DOI 10.1074/jbc.M504229200

Sébastien Dutertre‡§, Annette Nicke¶§‖, and Richard J. Lewis‡**

From the ‡Institute for Molecular Bioscience, The University of Queensland, Queensland 4072, Australia and the ¶Max Planck Institute for Experimental Medicine, Hermann Rein-Strasse 3, 37075 Göttingen, Germany

The structures of acetylcholine-binding protein (AChBP) and nicotinic acetylcholine receptor (nAChR) homology models have been used to interpret data from mutagenesis experiments at the nAChR. However, little is known about AChBP-derived structures as predictive tools. Molecular surface analysis of nAChR models has revealed a conserved cleft as the likely binding site for the 4/7 α-conotoxins. Here, we used an α3β2 model to identify β2 subunit residues in this cleft and investigated their influence on the binding of α-conotoxins MII, PnIA, and GID to the α3β2 nAChR by two-electrode voltage clamp analysis. Although a β2-L119Q mutation strongly reduced the affinity of all three α-conotoxins, β2-F117A, β2-V109A, and β2-V109G mutations selectively enhanced the binding of MII and GID. An increased activity of α-conotoxins GID and MII was also observed when the β2-F117A mutant was combined with the α4 instead of the α3 subunit. Investigation of A10L-PnIA indicated that high affinity binding to β2-F117A, β2-V109A, and β2-V109G mutants was conferred by amino acids with a long side chain in position 10 (PnIA numbering). Docking simulations of 4/7 α-conotoxin binding to the α3β2 model supported a direct interaction between mutated nAChR residues and α-conotoxin residues 6, 7, and 10. Taken together, these data provide evidence that the β subunit contributes to α-conotoxin binding and selectivity and demonstrate that a small cleft leading to the agonist binding site is targeted by α-conotoxins to block the nAChR.

Neuronal nicotinic acetylcholine receptors (nAChRs)[1] comprise a large family of ion channels formed by the heteropentameric assembly of homologous subunits. α-Conotoxins, small disulfide-rich peptides isolated from the venom of predatory cone snails, potently and selectively block nAChRs (1). They act as competitive antagonists at the ACh binding site, which is formed at the interface between neighboring subunits. These α-conotoxins can distinguish between muscle and neuronal nAChRs subtypes and even between different binding sites within the same receptor. As a result, they are widely used as pharmacological tools for the subtype differentiation of nAChRs in native tissues (2).

The 4/7 (4 residues in loop 1 and 7 in loop 2) α-conotoxins are of particular interest given their ability to discriminate between diverse neuronal α-β nAChR subunit combinations. For example, MII was found to be selective for the α3 and especially the α6 subunit containing nAChRs (3, 4) and aided the identification of the nAChR subunit composition in monkey striatum implicated in Parkinson disease (5, 6). The 4/7 α-conotoxin PnIA preferentially blocks α3β2 but also α7 rat nAChRs (7, 8), whereas α-GID potently blocks α7 and α3β2 nAChRs but also acts at α4β2 nAChR at higher concentrations (9). MII, PnIA, and GID share an identical backbone structure common to all 4/7 α-conotoxins investigated (9–11). Therefore, their specific selectivities are thought to arise from their different amino acid side chains. As a consequence, understanding the molecular determinants of their interaction with the receptor may help in the design of optimized pharmacological tools for the nAChRs with novel or improved selectivities. However, the lack of detailed information on the three-dimensional structure of the α-conotoxin binding site has hampered such projects.

The acetylcholine-binding protein (AChBP) crystal structure solved by Sixma and colleagues (12) recently provided a template to create homology models of the ligand binding domain of receptor members of the Cys-loop ligand-gated ion channels family. Homology models of the ligand binding domain of α7, α3β2, α3β4, and α4β2 nAChR subtypes are already providing useful insights into ligand-receptor interactions at the molecular level (13–16). Our previous docking simulations of α-conotoxins ImI and PnIB on an α7 nAChR homology model revealed that these two peptides target a small cleft forming one of two possible entrances to the ACh binding site (17). We could also identify an equivalent cleft on an α3β2 model as the likely region of the α3β2 nAChR targeted by these peptides. Upon examination of this model, it was apparent that the β2 subunit contributed more than the α subunit to the formation of this cleft, suggesting an important role of β-residues for binding and/or selectivity. In this study, we mutated three residues in the β2 subunit residues located in this cleft to characterize the contribution of the β subunit to α-conotoxin binding. Each of these mutants influenced the binding of α-conotoxins MII, GID, and PnIA. Additionally, molecular surface analysis revealed striking shape complementarity between the highly conserved N-terminal half of the 4/7 α-conotoxins structure and the cleft. Finally, docking experiments showed that both MII and PnIA bind deep into the α3β2 nAChR cleft, explaining at the molecular level the experimental results obtained from mutagenesis studies. Based on these results, we propose that the conserved cleft above the β9β10 hairpin is the binding site for 4/7 α-conotoxins active at α7, α3β2, and α4β2 nAChRs and that the

* This work was supported by Grant DP0208295 from the Australian Research Council, Grant NI 592/3-1 from the Deutsche Forschungsgemeinschaft, and a postgraduate scholarship from The University of Queensland (to S. D.). The costs of publication of this article were defrayed in part by the payment of page charges. This article must therefore be hereby marked "*advertisement*" in accordance with 18 U.S.C. Section 1734 solely to indicate this fact.

§ These authors contributed equally to this work.

‖ Current address: Max Planck Institute for Brain Research, Deutschordenstr. 46, D-60528 Frankfurt, Germany.

** To whom correspondence should be addressed: Inst. for Molecular Bioscience, University of Queensland, Brisbane, Queensland 4072, Australia. Tel.: 61-7-3346-2984; Fax: 61-7-3346-2101; E-mail: r.lewis@imb.uq.edu.au.

[1] The abbreviations used are: nAChR, nicotinic acetylcholine receptor; ACh, acetylcholine; AChBP, acetylcholine-binding protein.

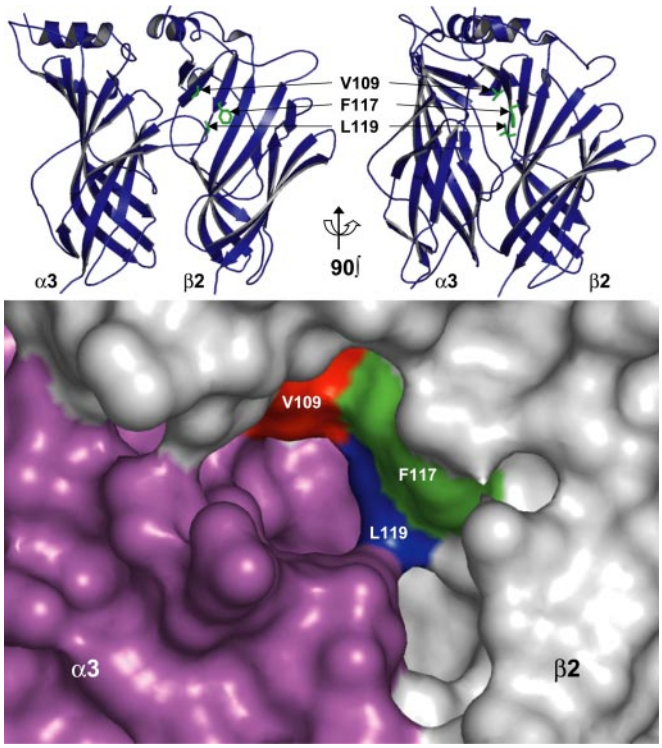

FIG. 1. **Homology model of the α3β2 nAChR showing the location of residues mutated in this study.** *A*, ribbon representation of α3β2 nAChR homology model with mutated residues in stick representation. *B*, enlarged view of the molecular surface of the α3/β2 subunit interface showing the relative contribution of both α3 (*purple*) and β2 (*white*) subunits to the cleft. Mutated residues are indicated.

differences in the cleft residues provide the determinants directing α-conotoxin selectivity.

EXPERIMENTAL PROCEDURES

Materials—cDNAs encoding neuronal nAChRs were provided by J. Patrick (Baylor College of Medicine, Houston, TX) and subcloned into the oocyte expression vector pNKS2 (18). MII, PnIA, and GID were gifts from J. T. Blanchfield (School of Pharmacy, The University of Queensland, Australia), G. Hopping and M. Loughnan (Institute for Molecular Bioscience, The University of Queensland, Australia), respectively, and were synthesized as described previously (9, 19, 20).

Homology Modeling—The FASTA format of the α3 and β2 rat sequences were retrieved from the ligand-gated ion channel data base (pasteur.fr/recherche/banques/LGIC/). Their extracellular ligand-binding domains were aligned with the AChBP sequence as described previously (21).

A homology model of the α3β2 nAChR subtype was built on a Silicon Graphics Octane R12000 work station using the MODELLER program (22). The AChBP structure (1I9B) was loaded in the INSIGHT II (Accelrys, San Diego, CA) environment and used as a template. Three models were built with a high "optimize level." The two options "optimize loop models" and "loop optimize level" were set to 3 and high, respectively. User disulfide was selected to assign the disulfide bonds as in AChBP except for the missing vicinal disulfide in the β2 subunit. The model with the lowest root mean square deviation compared with AChBP was refined further and used for these studies. Steepest descent energy minimizations were applied using the AMBER force field and DISCOVER program implemented in Insight II.

Mutagenesis—Mutagenesis of the β2 nAChR subunit cDNA was achieved using the QuikChange™ site-directed mutagenesis kit (Stratagene) following the manufacturer's instructions. Primers used to generate the mutants were from Proligo (Lismore, Australia). All mutations were confirmed by cDNA sequencing.

Electrophysiological Recordings—cRNA was synthesized from linearized plasmids with SP6 RNA polymerase using the mMessageMachine kit (Ambion, Austin, TX). *Xenopus laevis* frogs were purchased from Nasco International (Fort Atkinson, WI) or Firma Kähler (Hamburg, Germany). *X. laevis* oocytes were prepared as described previously (6) and injected with 50-nl aliquots of cRNA (0.5 μg/μl).

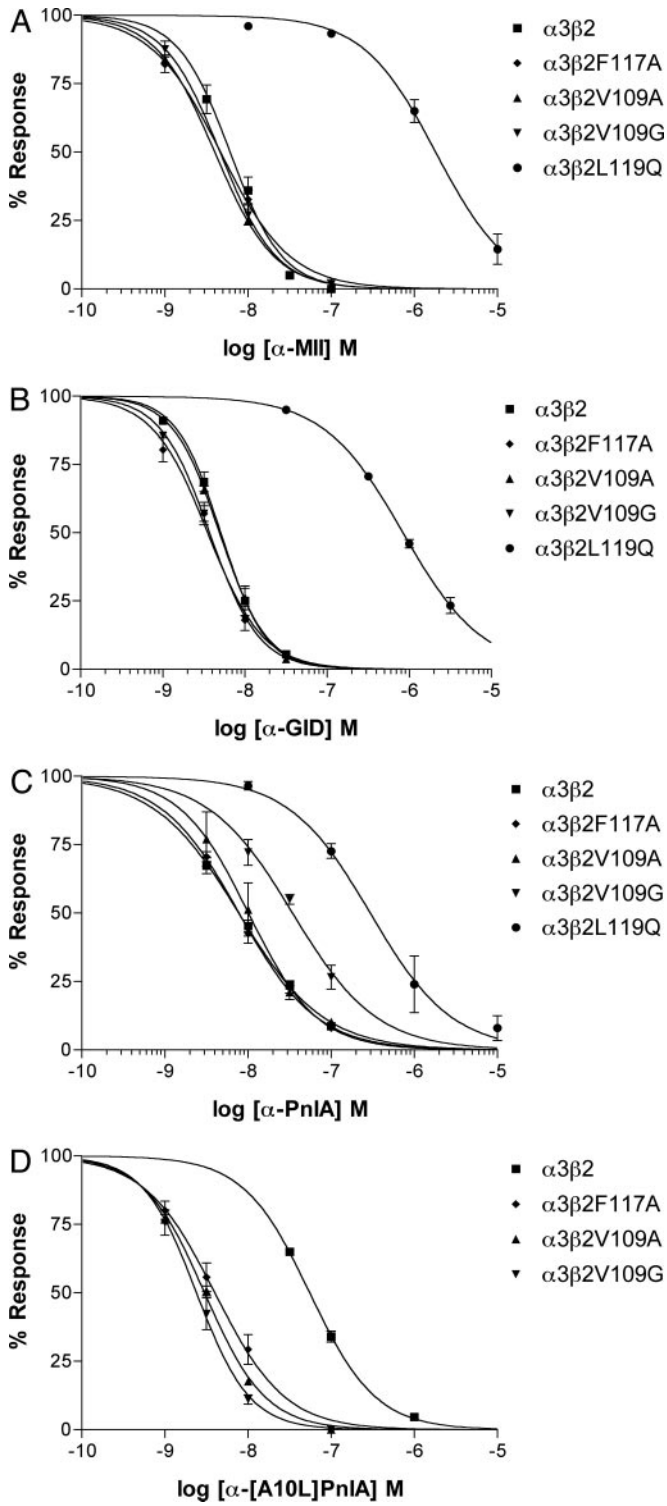

FIG. 2. **Concentration-response analysis of α-conotoxin MII (*A*), GID (*B*), PnIA (*C*), and [A10L]-PnIA (*D*) on wild type and mutant nAChRs.** The indicated subunit combinations were expressed in *Xenopus* oocytes and analyzed by 2-electrode voltage clamp. Responses to 2-s pulses of 100 μM ACh were recorded after a 3-min preincubation with the indicated toxin. IC_{50} values and Hill slopes are given in Table I. Each *point* represents the average of at least three measurements. *Error bars* represent S.E.

Two-electrode voltage clamp recordings were performed in oocytes 1–10 days after cRNA injection at a holding potential of −70 mV. Pipettes were pulled from borosilicate glass and filled with 3 M KCl. Resistances were below 1 megohm. Membrane currents were recorded using a Turbo Tec-10CX or a Turbo Tec 05X Amplifier (npi electronic, Tamm, Germany) filtered at 200 Hz and digitized at 400 Hz. Version

TABLE I
IC_{50} values and 95% confidence interval for α-conotoxins on wild type and mutant nAChR combinations

α-Conotoxins	IC_{50}		Hill slope	
	nM			
MII				
α3β2	6.08	(4.87–7.61)[b]	1.38	(0.94–1.83)
α3β2F117A	4.66	(3.59–6.05)	1.04	(0.80–1.27)
α3β2V109A	3.98	(3.58–4.43)	1.22	(1.10–1.33)
α3β2V109G	4.61	(3.70–5.75)	1.29	(1.01–1.56)
α3β2L119Q	1,810	(1,380–2,380)	0.99	(0.73–1.25)
GID				
α3β2	5.09	(4.17–6.22)	1.60	(1.11–2.10)
α3β2F117A	3.52	(2.81–4.42)	1.29	(0.90–1.68)
α3β2V109A	4.91	(4.39–5.48)	1.52	(1.26–1.78)
α3β2V109G	3.72	(3.27–4.22)	1.45	(1.18–1.71)
α3β2L119Q	839.20	(752.8–935.5)	0.90	(0.79–1.01)
PnIA				
α3β2	7.74	(6.79–8.81)	0.85	(0.74–0.97)
α3β2F117A	7.81	(6.71–9.08)	0.93	(0.79–1.07)
α3β2V109A	10.12	(7.11–14.43)	1.06	(0.64–1.47)
α3β2V109G	34.39	(26.47–44.68)	0.86	(0.60–1.12)
α3β2L119Q	295.80	(177.3–493.6)	0.88	(0.54–1.23)
[A10L]PnIA				
α3β2	55.23	(50.69–60.18)	1.09	(0.95–1.23)
α3β2F117A	3.99	(3.14–5.06)	1.03	(0.75–1.31)
α3β2V109A	3.00	(2.73–3.31)	1.19	(1.04–1.33)
α3β2V109G	2.40	(1.95–2.96)	1.36	(0.97–1.75)
MII				
α4β2	548.40	(400.6–750.7)	0.97	(0.69–1.25)
α4β2F117A	45.46	(31.38–65.84)	1.10	(0.72–1.49)
GID				
α4β2	390.00	(340.9–446.1)	1.31	(1.09–1.54)
α4β2F117A	58.73	(44.52–77.48)	1.35	(0.83–1.87)
PnIA				
α4β2	≫1000	ND[a]		
α4β2F117A	≫1000	ND		
α4β2V109A	≫1000	ND		
α4β2V109G	≫1000	ND		
[A10L]PnIA				
α4β2	≫1000	ND		
α4β2F117A	≫1000	ND		
α4β2V109A	≫1000	ND		
α4β2V109G	131.60	(101.4–170.9)	1.07	(0.78–1.36)

[a] ND, not determined.
[b] 95% confidence interval values are shown in parentheses.

TABLE II
Off-rate constants of α-conotoxins at wild type and mutant nAChR combinations

α-Conotoxins	k_{off}	
	min^{-1}	
MII		
α3β2	0.07	(0.04–0.1)[b]
α3β2F117A	ND[a]	(8.9 ± 0.7% recovery in 20 min)
α3β2V109A	ND	(11.4 ± 2.6% recovery in 20 min)
α3β2V109G	ND	(14.1 ± 2.5% recovery in 20 min)
GID		
α3β2	0.19	(0.15–0.22)
α3β2F117A	ND	(15.2 ± 3.0% recovery in 20 min)
α3β2V109A	0.09	(0.06–0.12)
α3β2V109G	0.03	(0.01–0.05)
PnIA		
α3β2	ND	(100% recovery in 2 min)
α3β2F117A	ND	(100% recovery in 4 min)
α3β2V109A	ND	(100% recovery in 4 min)
α3β2V109G	ND	(100% recovery in 2 min)
[A10L]PnIA		
α3β2	ND	(100% recovery in 2 min)
α3β2F117A	0.09	(0.07–0.11)
α3β2V109A	0.12	(0.09–0.15)
α3β2V109G	ND	(13.2 ± 3.3% recovery in 20 min)

[a] ND, not detectable.
[b] 95% confidence interval values are shown by numbers in parentheses.

8.53 Pulse software (HEKA Elektronik, Lambrecht, Germany) or CellWorks software were used. The perfusion medium was automatically switched between ND96 with or without agonist (100 μM ACh) using a custom-made magnetic valve system. A fast and reproducible solution exchange (<300 ms) for agonist application was achieved using a 50-μl funnel-shaped oocyte chamber combined with a fast solution flow (~150 μl/s) fed through a custom-made manifold mounted immediately above the oocyte. ACh pulses were applied for 2 s at 4-min intervals. After each application, the cell was superfused for 1 min with agonist-free solution, and the flow was then stopped for 3 min. Peptide was mixed from a 10-fold stock into the static bath when responses to three consecutive agonist applications differed by less than 10%. Addition of toxin directly to the recording chamber conserved material and avoided adhesion of the toxin to tubing surfaces. To obtain estimates of potency, dose-response curves were fit to the data by the equation % response = $100/\{1 + ([\text{toxin}]/IC_{50})^{nH}\}$ using Prism software (GraphPad version 3.0 for Macintosh, San Diego, CA). To obtain estimates of toxin dissociation rates, agonist responses were measured at 2-min intervals under constant superfusion, and after stabilization of responses, oocytes were incubated with toxin in a static bath for 1 min. To obtain estimates of the toxin association rate, oocytes were continuously superfused with solution containing the indicated toxin concentration and ACh pulses were applied in 1- or 2-min intervals. Association and dissociation curves were fit to the data by the equations % response = (100 − plateau) × $e^{-K \times \text{time}}$ + plateau and % response = span (1 − $e^{-K \times \text{time}}$) + plateau, respectively.

Docking Experiments—Docking simulations of α-conotoxins were carried out as described in Dutertre *et al.* (17). Briefly, MII and PnIA structures were retrieved from the protein data bank (Protein Data Bank codes 1MII and 1PEN, respectively) and docked onto an α3β2 homology model using the program GOLD, version 1.2 (Genetic Optimization for Ligand Docking, Cambridge Crystallographic Data Centre, Cambridge, UK). One NMR/crystal structure was chosen for each α-conotoxin, as GOLD treats ligands as flexible molecules with side chain orientations optimized during calculations. As conotoxins are competitive antagonists, the active site radius was set at 20 Å from

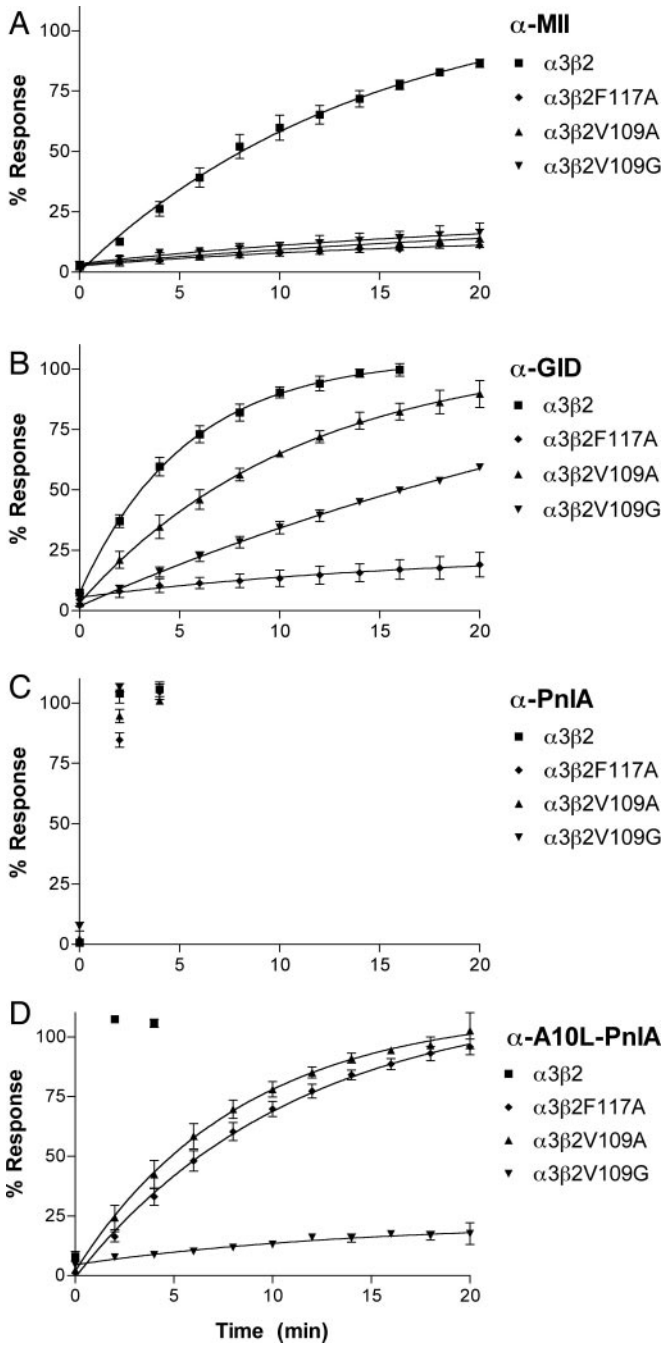

FIG. 3. **Off-rate kinetics of α-conotoxins MII (*A*), GID (*B*), PnIA (*C*), and [A10L]-PnIA (*D*) on wild type and mutant nAChRs.** Responses to 2-s pulses of ACh after a 90–100% block by the indicated toxins were recorded at 2-min intervals during continuous superfusion. Off-rate constants are given in Table II. Each *point* represents the average of at least three measurements. *Error bars* represent S.E.

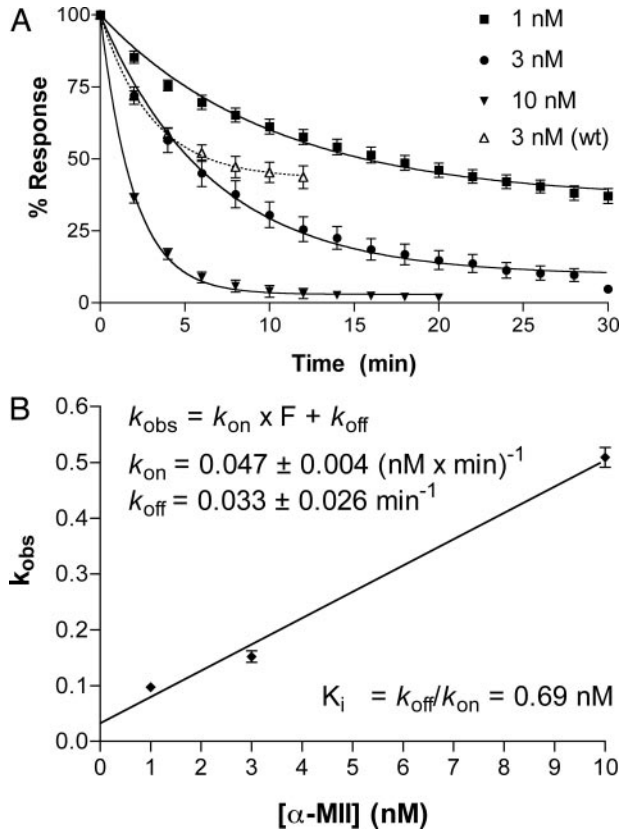

FIG. 4. **Experimentally determined on-rate kinetics and calculated off-rate constant of α-conotoxin MII at the α3β2F117A mutant nAChR.** *A*, the indicated concentrations of MII were applied by continuous perfusion to oocytes expressing the α3β2F117A mutant, and responses to 2-s pulses of ACh were monitored at 1- or 2-min intervals. The faster on-rate kinetics of MII at the wild type α3β2 receptor is shown for comparison. *B*, experimentally determined on-rate constants were plotted against the toxin concentration to obtain an estimate of the off-rate constant and the K_i value. *F* in the formula indicates the free toxin concentration. Each *point* represents the average of at least three measurements. *Error bars* represent S.E.

Trp-147 to ensure the analysis focused on residues around the ACh binding site. From the 100 docked structures obtained for each conotoxin, the selection of the final docked structure was based on a low scoring function determined in GOLD (23).

RESULTS AND DISCUSSION

Homology Modeling Identifies Val-109, Phe-117, and Leu-119 in the β2 nAChR Subunit as Likely Residues Interacting with α-Conotoxins MII and PnIA—We previously identified two cavities at opposite sides of the β9/10 hairpin (C-loop of an α subunit) on the surface of the nAChR, one large and easily accessible and one small and narrow, from which the ACh binding site could be reached (21). To differentiate between these two cavities and avoid confusion, we propose the use of "cavity" to refer to the larger one (below the β9β10 hairpin, close to the cell membrane), and "cleft" to refer to the smaller one (above the β9β10 hairpin). The cavity has recently been confirmed to represent the binding site used by the large snake neurotoxins to block the nAChR (24), whereas the cleft represents the likely region targeted by α-conotoxins (17, 21). Docking simulations with ImI and PnIB structures on an α7 nAChR model revealed overlapping but different binding sites for α-conotoxins and snake toxins (17). Both α-conotoxins block the receptor by targeting a small cleft above the β9/10 hairpin that is also blocked by the small peptide antagonist toxin waglerin (25) and the non-peptidic antagonist *d*-tubocurarine (26). Concerning the α3β2 nAChR, only one residue (β2-Thr-57) weakly affecting 4/7 conotoxin binding has been identified on the β2 subunit compared with four on the α3 subunit (27, 28). Interestingly, β2-Thr-57 is located above the β9β10 hairpin, forming part of the cleft in α3β2 together with three other residues, Val-109, Phe-117, and Leu-119. A potentially important role for additional residues in the β subunit is suggested from binding kinetic studies where exchange of the β2 subunit by the β4 subunit (in combination with α3 or α6 subunits) strongly reduced the off-rate constants of PIA (29). Likewise, BuIA showed much slower dissociation if α2, α3, α4, or α6 subunits are combined with β4 instead of β2 (30). In an attempt to identify additional determinants in the β subunit that contribute to the binding and selectivity of 4/7 α-conotoxins, we mu-

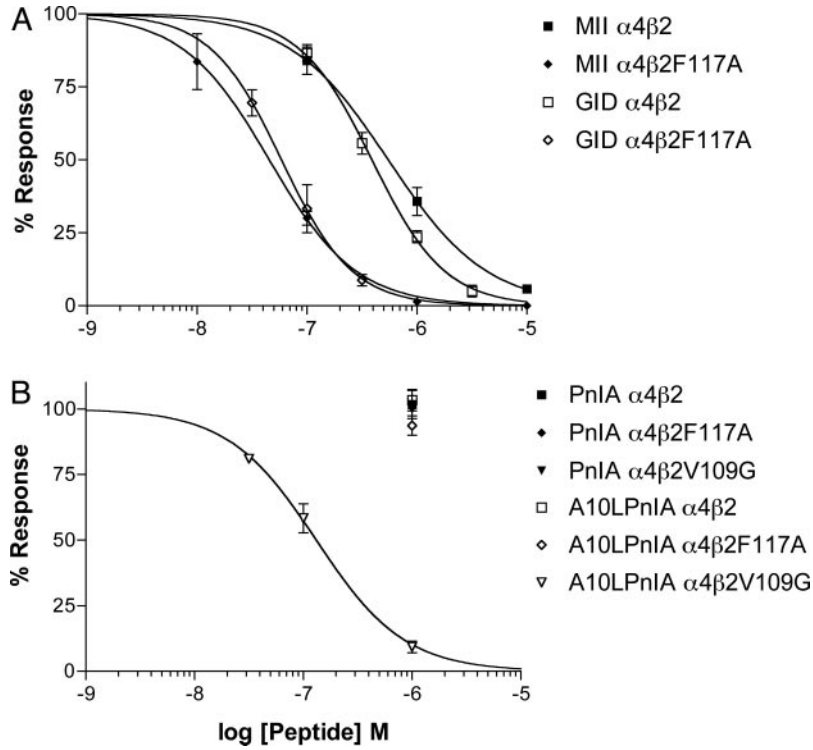

FIG. 5. **Activity of α-conotoxins MII and GID (*A*) and PnIA and [A10L]PnIA (*B*) on wild type and mutant α4β2 nAChRs.** The indicated subunit combinations were expressed in *Xenopus* oocytes, and responses to 2-s pulses of 100 μM ACh were recorded after a 3-min preincubation with different concentrations of the indicated toxin. IC_{50} values and Hill slopes are given in Table I. Each *point* represents the average of at least three measurements. *Error bars* represent S.E.

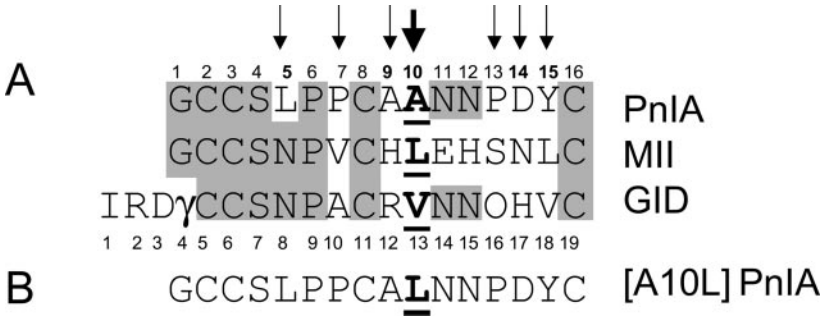

FIG. 6. **Sequence comparison of α-conotoxins acting at the α3β2 nAChR.** *A*, although MII and GID show an enhanced binding at the α3β2V109A/G and F117A mutants, the binding of PnIA appeared unchanged. Residues common to PnIA and MII and/or GID are marked in *gray*. Residues indicated by *arrows* could account for the observed differences. *B*, L10A exchange in PnIA enhanced binding of PnIA at the mutants, indicating that a long or bulky aliphatic side chain in position 10 conferred a strong interaction with the β2-F117A and β2-V109G/V109A mutants.

tated Leu-119, which appears deep in the cleft, as well as Phe-117 and Val-109, which form part of the wall of the cleft (Fig. 1).

Residue Leu-119 Is Generally Important for α-Conotoxin Binding—A leucine in position β2-119 lies at the bottom of the cleft and is conserved in neuronal β4 and α7 nAChR subunits as well as in the muscle δ, γ, and ε nAChR subunits. Thus, a leucine is present at this location in all non-α subunits (and the (−) face of the α7 nAChR) for which highly active α-conotoxins have been identified. Indeed, no potent α-conotoxin has been found for the α9 and α10 subunits, which have a negatively charged aspartic acid at this position. In combination with the docking studies, this suggests that the hydrophobic environment created by β2-Leu-119 and the corresponding leucine residues in other subunits plays an important role in the high affinity interaction with α-conotoxins. To test the hypothesis that Leu-119 is generally important for α-conotoxin binding, the activity of three different α-conotoxins that bind with high affinity to the α3β2 nAChRs was tested on the hydrophilic α3β2-L119Q mutant. The α3β2/α6β2-selective α-conotoxin MII as well as the α3β2/α7-selective α-conotoxins PnIA and GID had a strongly reduced activity (Fig. 2, *A–C*), with 40-fold (PnIA), 165-fold (GID), and 300-fold (MII) higher IC_{50} values at this mutant α3β2 receptor (Table I). This is the strongest effect described thus far for a non-α subunit mutant affecting α-conotoxin binding. Based on its position at the bottom of the cleft and the fact that the activity of all three conotoxins was reduced by at least 40-fold upon introduction of a similar length hydrophilic residue (Gln), Leu-119 may play an important stabilizing role for the interaction with α-conotoxins, allowing them to bind deep into the nAChR cleft.

In addition to the four cysteines, which are involved in two disulfide bonds and are mostly buried within the peptide core, only serine and proline residues are common to all three α-conotoxins. Because mutation of Ser-4 in MII did not affect potency (31), we suspect that Leu-119 might interact with the α-conotoxin backbone or the conserved proline found in 4/7 α-conotoxins (third residue of loop 1). However, this possibility is difficult to test by double mutant cycle analysis because alteration of the conserved cysteine or proline residues in the conotoxin alters the peptide backbone conformation.

Alanine Exchange of Val-109 and Phe-17 Specifically Enhances Binding of MII and GID—In our model of the β2 subunit, residues Val-109 and Phe-117 lie adjacent to each other on two neighboring antiparallel β-strands and above the Leu-119 residue, potentially forming the walls of the α-conotoxin binding cleft (Fig. 1). By mutating the residues into the smaller alanine, we expected to weaken the interaction with α-conotoxins. Unexpectedly, both the F117A and V109A mutations produced IC_{50} values for MII, GID, and PnIA little different from those at the wild type receptor, suggesting that Phe-117 and Val-109 do not have close interactions with the α-conotoxins

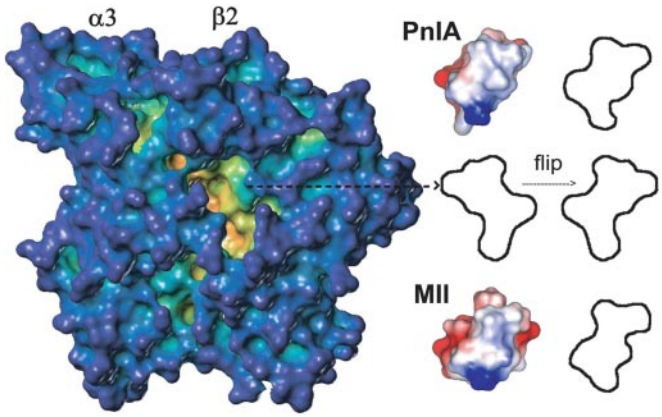

FIG. 7. **Molecular surface complementarities for α-conotoxins and the α3β2 cleft.** Molecules are shown at the same scale, allowing direct size comparison and shape complementarity between α-conotoxins and the nAChR cleft. α-Conotoxins PnIA and MII are shown with their N-terminal sequences facing the reader. The contour of the cleft was flipped 180° to allow a direct comparison with the α-conotoxin shapes. This figure was produced using MOLCAD in Sybyl7.0 (Tripos software, St. Louis, MO).

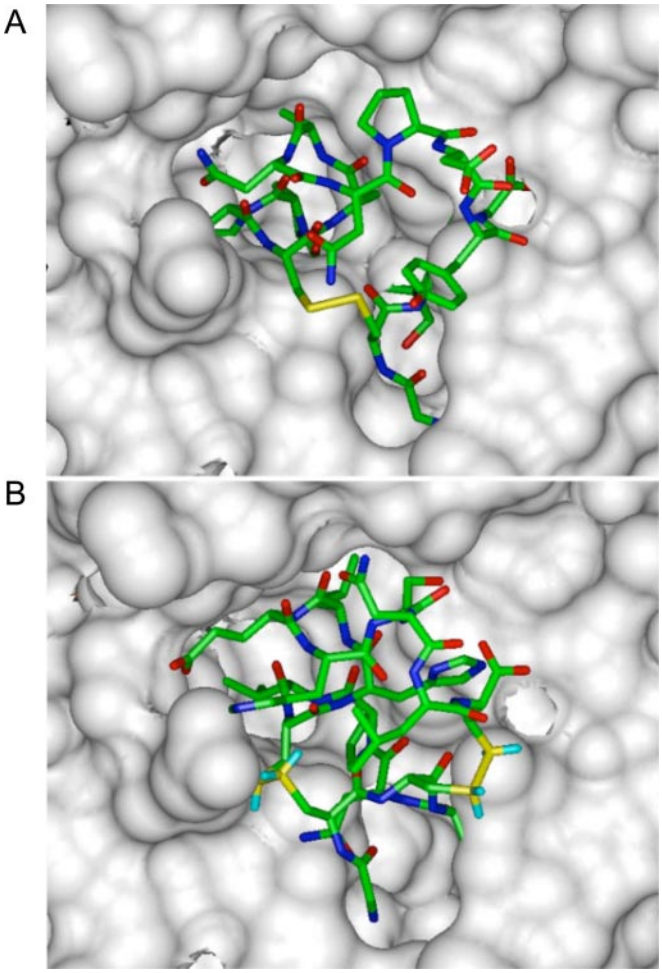

FIG. 8. **Docking of PnIA (*A*) and MII α-conotoxins (*B*) onto the α3β2 nAChR.** Each of these conotoxins penetrated deep into the cleft with its conserved N-terminal hydrophobic patch, which includes the conserved Pro-6. Toxin residues make contacts with both the α3 and β2 subunits. The C-terminal part of both conotoxins protrudes beyond the cleft.

(Fig. 2, *A–C*, Table I). The same effect was observed for V109G (except for PnIA, where a slight decrease in affinity was observed). However, the off-rates of MII were affected by all three mutations (Table II), resulting in a very slowly reversible block by MII (Fig. 3*A*). A similar effect on the binding was observed with GID (Fig. 3*B*). In contrast, the off-rates of PnIA appeared to be hardly affected by the mutations (Fig. 3*C*). The finding that alanine exchange of Val-109 or Phe-117 decreased the off-rate constants of MII and GID without an obvious change in the IC_{50} value implied that a similar reduction in on-rate had occurred to balance the off-rate change or that the IC_{50} value had not been determined accurately because of the short 3-min preincubation times. To obtain a more accurate estimate of the potency, on-rates of MII binding to the wild type and F117A mutant were compared. As expected, the F117A mutant displayed a much slower on-rate for MII compared with its on-rate at the wild type receptor (Fig. 4*A*). Calculated on- and off-rates for MII at the α3β2F117A mutant produced a K_i value of 0.69 nM (Fig. 4*B*), ~ 10-fold lower than the experimentally determined IC_{50} value (Fig. 2*A*, Table I). Unfortunately, the long incubation times necessary to determine the real IC_{50} values at the α3β2F117A and Val-109 mutants were not practical because of run-up/down effects on nAChR current seen in oocytes and the large amounts of toxin needed for superfusion. Therefore, to complement the IC_{50} value determinations, we compared off-rates as a measure of toxin affinity that is independent of toxin concentration or preincubation time. Because not only the off-rate constants but also the on-rate constant of GID and MII on the Val-109 and Phe-117 mutants were decreased, we propose that these residues comprise part of a short access path or an intermediate binding state that α-conotoxins transition past before reaching (or leaving) their high affinity bound state.

The Effect on Val-109 and Phe-117 Exchange Also Occurs in Combination with the α4 nAChR Subunit—The results presented above show that a small modification of the β2 subunit can have a strong and specific effect on conotoxin binding, suggesting that the β subunit contributes to α-conotoxin binding through direct and specific interactions. However, it cannot be excluded that this is a secondary effect because of an alteration in the conformation of the α subunit induced by the mutation in the β subunit. To address this aspect, we investigated whether these β2 effects were preserved in combination with a different α subunit. Both MII and GID showed nanomolar activity at the α4β2 nAChR subtype, whereas no activity was observed for PnIA at concentration up to 1 μM. When the α4 subunit was combined with the β2-F117A mutation, both GID and MII showed an ~10-fold increase in activity (Fig. 5*A*) that was likewise paralleled by a clearly decreased off-rate (results not shown). This further indicates that the binding modes of MII and GID within the binding pocket are conserved across the α4β2 and α3β2 receptor interfaces and that the β subunit contributes directly to α-conotoxin potency. Whereas the overall higher IC_{50} values at the α4β2 combination suggest that the contribution of the α4 subunit to conotoxin binding is smaller than that of the α3 subunit, the inactivity of PnIA could also be explained by a residue in PnIA that prevents an interaction with the α4 subunit.

The Length of the Side Chains in Position 10 of the α-Conotoxins Determines the Strength of the Interaction with the Val-109 and Phe-117 Mutants—Sequence comparison of PnIA with MII and GID (Fig. 6) shows that there are 7 residues in PnIA (Leu-5, Pro-7, Ala-7, Ala-10, Pro-13, Asp-14, and Tyr-15), which are different from the corresponding residues in GID or MII and thus are likely candidates to account for the poor activity of PnIA at the α4β2 interface and the low affinity of PnIA (compared with GID and MII) at the α3β2 mutants. Because MII has a leucine and PnIA an alanine at position 10, it appears that a long or bulky aliphatic side chain enhances α-conotoxin

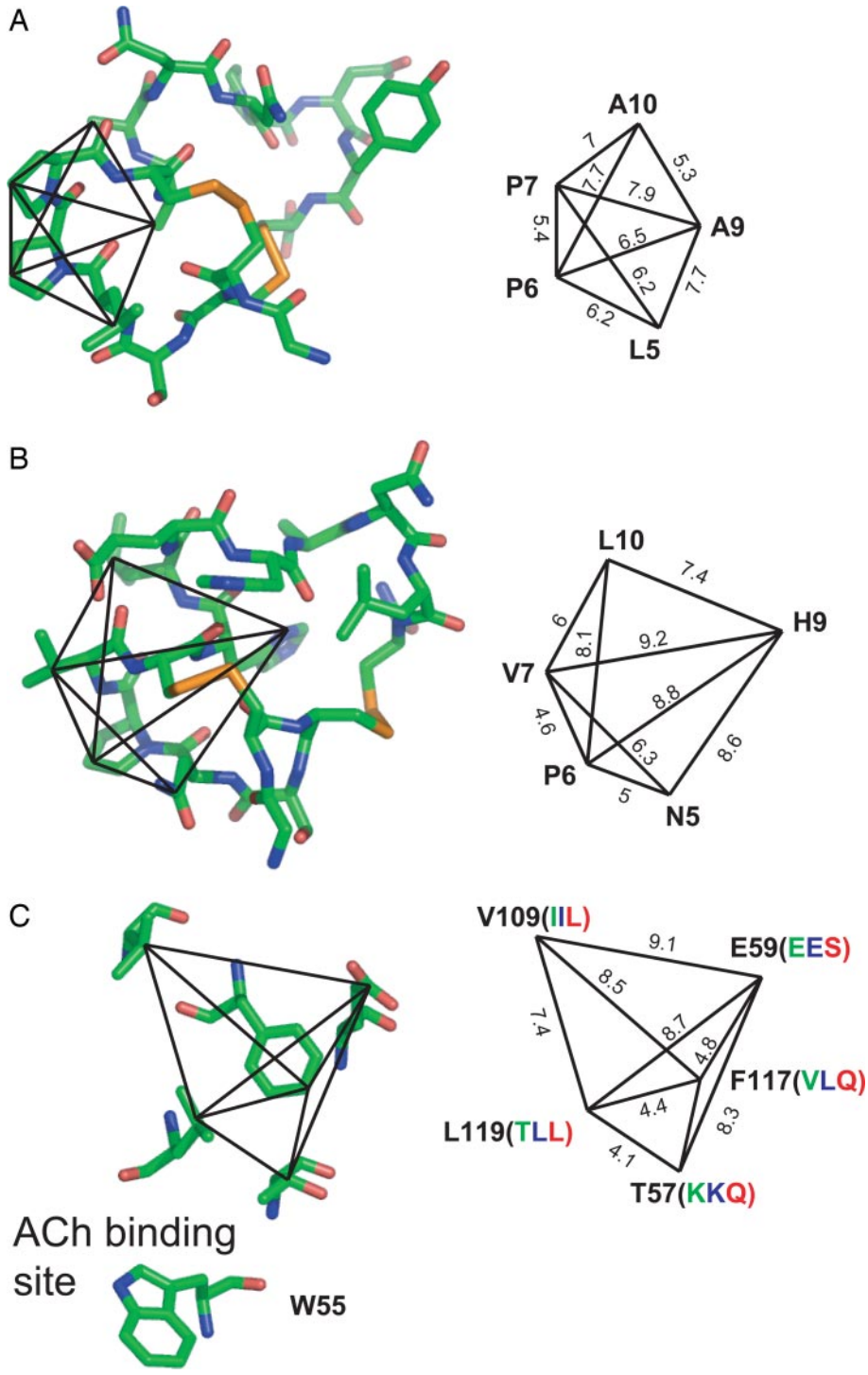

FIG. 9. **α-Conotoxin and β2 subunit pharmacophores.** PnIA (*A*) and MII (*B*) conotoxins are presented in their docked orientation in the cleft (*C*). The minimal pharmacophore shown is consistent with mutagenesis results and previous α-conotoxin alanine scan data. Distances (Å) between residues are measured from the last carbon of the side chain and reported on the vectors in the *right-hand panels*. Also shown are the equivalent residues for the β3 (*green*), β4 (*blue*), and (−) α7 (*red*) subunits. Note that Phe-117 is positioned under Glu-59.

interactions with the Phe-117 and Val-109 mutants. To further test this hypothesis, we investigated the activity of the A10L-PnIA analogue on both α3β2 and α4β2 mutants. As predicted, replacing Ala-10 by a longer leucine residue enhanced PnIA affinity for β2 receptors containing the Phe-117 or Val-109 mutations (Figs. 2*D* and 3*D*; Tables I and II). Indeed, a markedly reduced off-rate constant and an up to 23-fold lower IC_{50} value were observed for A10L-PnIA at the β2 mutants (Table I: 3.99 nM on β2-F117A; 3 nM on β2-V109A; 2.4 nM on β2-V109G) compared with the wild type α3β2 receptor (55 nM). Moreover, this A10L modification converted PnIA into a potent antagonist at the α4β2-V109G receptor (Fig. 5*B*).

Residue 10 in PnIA has previously been shown to be an important determinant of selectivity between α3β2 and α7 receptors (8). A comparison of a range of conotoxins with sequence similarity in the second loop showed that the length of the side chain in position 10 correlated with an α7 *versus* α3β2 selectivity. This correlation was also found to be valid for GID and PnIA but not for MII, suggesting that MII has an altered binding mode. However, the similar influence of β2 mutants on GID, PnIA, and MII affinity indicate that these 4/7 α-conotoxins orientate similarly within the cleft formed by the α/β interface and that the critical position 10 side chain likely faces the β2 subunit in all three α-conotoxins.

Shape and Size Complementarity between 4/7 α-Conotoxins and the Cleft in nAChRs—A high affinity complex requires either a large contact area between receptor and ligand surfaces with multiple points of interaction *or* shape complemen-

tarity that favors the formation of a smaller number of specific interactions (*e.g.* a ligand bound in a protein cleft). Given their relatively small size, the high affinity complex observed for α-conotoxins suggests that a tight fit between the α-conotoxin and a cleft on the nAChR surface is likely to occur. The α7 nAChR cleft appears to be ~7 Å deep, 13.5 Å long, and 9.5 Å wide (6.6 Å at the narrowest point). These dimensions are almost identical to those found for the α3β2 nAChR (7.5 Å deep, 14.5 Å long, and 9.8 Å wide (6.8 Å at the narrowest)), and are mostly conserved in shape. For comparison, we measured the dimensions of the N-terminal hydrophobic patch of α-conotoxins. In MII it is 12 Å long (Gly- to Val-7) and 7 Å wide, and in PnIA it is 11.2 Å long (Gly-1 to Pro-7) and 6.5 Å wide, whereas GID has a flexible tail that complicates the measurements (a tail-truncated analogue has similar dimension to PnIA and MII, and the tail could be accommodated by the flexible loop F of nAChR). These comparisons reveal a striking size and shape complementarity between 4/7 α-conotoxins and the nAChR cleft, strongly suggesting a lock-and-key interaction (Fig. 7).

Docking Models of PnIA and MII Interactions with α3β2 nAChR—To verify that 4/7 α-conotoxins can interact with the nAChR cleft via their conserved hydrophobic patch (residues 6, 7, and 10), docking of PnIA and MII structures onto an α3β2 nAChR model were simulated using the program GOLD. Analysis of the results from docking simulations confirmed both hypotheses: the small cleft is the binding site for 4/7 α-conotoxins, and the α-conotoxins bind to the α3β2 nAChR by presenting their conserved N-terminal shape (Fig. 7). Indeed, although an active site radius set to 20 Å would have allowed ligands to dock at other locations around the C-loop, all structures were found docked in the cleft above the β9/10 hairpin. The final orientation of PnIA and MII docked into the receptor cleft presented in Fig. 8 was chosen from the cluster of lowest energy structures produced by GOLD and on the basis of how well it fitted the available experimental data. Both α-conotoxins bind in a similar way to the docking mode found for PnIB at the α7 nAChR (17). It is interesting to note that although MII still binds to α3β2 from its hydrophobic patch similarly to PnIA, its position in the cleft appears slightly shallower compared with PnIA, as expected given the greater width of its C-terminal half (see Fig. 7). Interestingly, MII is observed to make additional contacts with α3β2 nAChR residues, giving an explanation for its very slow off-rate and associated higher affinity compared with PnIA. Indeed, although β2-L119 appears in close proximity to the conserved P6 residue, and position 10 residues are found between β2-V109 and β2-F117 in both PnIA and MII, only His-9 of MII makes an electrostatic interaction with β2-Glu-57 possible. However, the hydrophobic interaction between α-conotoxins (positions 6, 7, and 10) and the nAChR cleft (Leu-119, Val-109 and Phe-117) appears to play a significant role in the high affinity complex observed. Mutagenesis experiments carried out by others have identified 5 residues influencing MII and PnIA binding (27, 28). Although β2-Thr-57 is located in the cleft, and α3-Ile-183 is in close proximity of both docked structures, residues Lys-183, Pro-180, and Gln-196 are far from the binding site. We propose that their effect on peptide binding is likely to be indirect, as they are all located on the structurally important β9/10 hairpin and include two proline mutants (P180T and Q196P), expected to have a significant structural effect. The orientation of 4/7 α-conotoxins in the cleft explains the functional data obtained from the β2 mutants.

Pharmacophore—We developed a minimal antagonist pharmacophore for 4/7 α-conotoxins based on our mutagenesis and docking results (Fig. 9). PnIA has a very hydrophobic N-terminal patch, comprising Leu-5, Pro-6, Pro-7, Ala-9, and Ala-10 (Fig. 9*A*). MII also possesses a similar hydrophobic core (Pro-6, Val-7, and Leu-10) that we take to represent a minimum antagonist pharmacophore (Fig. 9*B*). When compared with the β2 subunit pharmacophore (Fig. 9*C*), the distances found in conotoxins are compatible with the direct interaction between the conserved proline in position 6 and β2-Leu-119 that we observed in our docking model. We propose that Pro-6 in 4/7 conotoxin acts as an anchor and stabilizes the conotoxin-receptor complex. Additional hydrophobic contacts such as Pro-7 (PnIA) or Val-7 (MII) and Ala-10 (PnIA) or Leu-10 (MII) with β2-Val-109 and β2-Phe-117 strengthen the interaction, whereas secondary interactions such as His-9 (MII) and β2-Glu-57 determine the selectivity. A comparison of residues in the equivalent position of the receptor pharmacophore in other β subunits and (−) α7 reveals important differences likely to influence α-conotoxin selectivity (Fig. 9*C*). For example, the polar Thr-119 residue present in β3 may explain the absence of α-conotoxins acting at nAChRs containing this subunit.

Conclusions—We have demonstrated the predictiveness of nAChR homology models based on the AChBP structure and characterized a small cleft as the common binding site for 4/7 α-conotoxins. Point mutations in this cleft revealed a major effect of β2-Leu-119 on α-conotoxin affinity and important influences of β2-Phe-117 and β2-Val-109 on α-conotoxin binding kinetics. Furthermore, we could demonstrate a specific interaction of residue 10 in α-conotoxins with the β2 subunit. Docking simulations of PnIA and MII at α3β2 confirmed these results by showing a direct interaction between β2 and α-conotoxin residues. These studies indicate that α-conotoxins block the nAChRs by a lock-and-key interaction, where a primary hydrophobic interaction between β2-Leu-119 and the conserved Pro of 4/7 α-conotoxins "locks" the ligand in its cleft, and secondary complementary interactions contribute to ligand selectivity. Based on homology models of nAChRs, the identification of ligand-accessible residues in the cleft (Leu-119, Val-109, and Phe-117) and the determination of a minimal antagonist pharmacophore, a rational approach to the design of subtype-selective nAChR modulators can now be pursued.

Acknowledgments—We thank Joanne T. Blanchfield, Gene Hopping, and Marion Loughnan for the gifts of MII, PnIA, and GID, respectively, Jim Patrick for providing the nAChR cDNAs, Benjamin Marquez-Klaka for help with the RNA synthesis, Jürgen Rettinger for helpful discussion, and Paul Alewood, Florentina Soto, Walter Stühmer, and Heinrich Betz for generous support.

Note Added in Proof—Our studies on 4/7 α-conotoxin binding mode at mammalian nAChRs are strikingly similar to the binding mode determined for 4/7 α-conotoxins co-crystallized with AChBP (Celie, P. H., Kasheverov, I. E., Mordvintsev, D. Y., Hogg, R. C., van Nierop, P., van Elk, R., van Rossum-Fikkert, S. E., Zhmak, M. N., Bertrand, D., Tsetlin, V., Sixma, T. K., and Smit, A. B. (2005) *Nat. Struct. Mol. Biol.*, in press), revealing a remarkable conservation of α-conotoxin binding to nAChRs across different species and subtypes. Interestingly, AChBP has a Met instead of the equivalent Leu-119 in β2 that contributes to the binding of α-conotoxins.

REFERENCES

1. McIntosh, J. M., Santos, A. D., and Olivera, B. M. (1999) *Annu. Rev. Biochem.* **68,** 59–88
2. Nicke, A., Wonnacott, S., and Lewis, R. J. (2004) *Eur. J. Biochem.* **271,** 2305–2319
3. Kuryatov, A., Olale, F., Cooper, J., Choi, C., and Lindstrom, J. (2000) *Neuropharmacology* **39,** 2570–2590
4. Vailati, S., Hanke, W., Bejan, A., Barabino, B., Longhi, R., Balestra, B., Moretti, M., Clementi, F., and Gotti, C. (1999) *Mol. Pharmacol.* **56,** 11–19
5. Salminen, O., Murphy, K. L., McIntosh, J. M., Drago, J., Marks, M. J., Collins, A. C., and Grady, S. R. (2004) *Mol. Pharmacol.* **65,** 1526–1535
6. Quik, M., Polonskaya, Y., Kulak, J. M., and McIntosh, J. M. (2001) *J. Neurosci.* **21,** 5494–5500
7. Luo, S., Nguyen, T. A., Cartier, G. E., Olivera, B. M., Yoshikami, D., and McIntosh, J. M. (1999) *Biochemistry* **38,** 14542–14548
8. Hogg, R. C., Miranda, L. P., Craik, D. J., Lewis, R. J., Alewood, P. F., and Adams, D. J. (1999) *J. Biol. Chem.* **274,** 36559–36564
9. Nicke, A., Loughnan, M. L., Millard, E. L., Alewood, P. F., Adams, D. J., Daly,

N. L., Craik, D. J., and Lewis, R. J. (2003) *J. Biol. Chem.* **278,** 3137–3144
10. Hill, J. M., Oomen, C. J., Miranda, L. P., Bingham, J. P., Alewood, P. F., and Craik, D. J. (1998) *Biochemistry* **37,** 15621–15630
11. Hu, S. H., Gehrmann, J., Guddat, L. W., Alewood, P. F., Craik, D. J., and Martin, J. L. (1996) *Structure* **4,** 417–423
12. Brejc, K., van Dijk, W. J., Klaassen, R. V., Schuurmans, M., van Der Oost, J., Smit, A. B., and Sixma, T. K. (2001) *Nature* **411,** 269–276
13. Le Novere, N., Grutter, T., and Changeux, J. P. (2002) *Proc. Natl. Acad. Sci. U. S. A.* **99,** 3210–3215
14. Schapira, M., Abagyan, R., and Totrov, M. (2002) *BMC Struct. Biol. 2002* **2,** 1
15. Fruchart-Gaillard, C., Gilquin, B., Antil-Delbeke, S., Le Novere, N., Tamiya, T., Corringer, P. J., Changeux, J. P., Menez, A., and Servent, D. (2002) *Proc. Natl. Acad. Sci. U. S. A.* **99,** 3216–3221
16. Samson, A., Scherf, T., Eisenstein, M., Chill, J., and Anglister, J. (2002) *Neuron* **35,** 319–332
17. Dutertre, S., Nicke, A., Tyndall, J. D., and Lewis, R. J. (2004) *J. Mol. Recognit.* **17,** 339–347
18. Gloor, S., Pongs, O., and Schmalzing, G. (1995) *Gene* **160,** 213–217
19. Blanchfield, J. T., Dutton, J. L., Hogg, R. C., Gallagher, O. P., Craik, D. J., Jones, A., Adams, D. J., Lewis, R. J., Alewood, P. F., and Toth, I. (2003) *J. Med. Chem.* **46,** 1266–1272
20. Hogg, R. C., Hopping, G., Alewood, P. F., Adams, D. J., and Bertrand, D. (2003) *J. Biol. Chem.* **278,** 26908–26914
21. Dutertre, S., and Lewis, R. J. (2004) *Eur. J. Biochem.* **271,** 2327–2334
22. Sali, A., and Blundell, T. L. (1993) *J. Mol. Biol.* **234,** 779–815
23. Jones, G., Willett, P., Glen, R. C., Leach, A. R., and Taylor, R. (1997) *J. Mol. Biol.* **267,** 727–748
24. Bourne, Y., Talley, T. T., Hansen, S. B., Taylor, P., and Marchot, P. (2005) *EMBO J.*, in press
25. Molles, B. E., Tsigelny, I., Nguyen, P. D., Gao, S. X., Sine, S. M., and Taylor, P. (2002) *Biochemistry* **41,** 7895–7906
26. Gao, F., Bern, N., Little, A., Wang, H. L., Hansen, S. B., Talley, T. T., Taylor, P., and Sine, S. M. (2003) *J. Biol. Chem.* **278,** 23020–23026
27. Everhart, D., Reiller, E., Mirzoian, A., McIntosh, J. M., Malhotra, A., and Luetje, C. W. (2003) *J. Pharmacol. Exp. Ther.* **306,** 664–670
28. Harvey, S. C., McIntosh, J. M., Cartier, G. E., Maddox, F. N., and Luetje, C. W. (1997) *Mol. Pharmacol.* **51,** 336–342
29. Dowell, C., Olivera, B. M., Garrett, J. E., Staheli, S. T., Watkins, M., Kuryatov, A., Yoshikami, D., Lindstrom, J. M., and McIntosh, J. M. (2003) *J. Neurosci.* **23,** 8445–8452
30. Azam, L., Dowell, C., Watkins, M., Stitzel, J. A., Olivera, B. M., and McIntosh, J. M. (2005) *J. Biol. Chem.* **280,** 80–87
31. Everhart, D., Cartier, G. E., Malhotra, A., Gomes, A. V., McIntosh, J. M., and Luetje, C. W. (2004) *Biochemistry* **43,** 2732–2737

β2 Subunit Contribution to 4/7 α-Conotoxin Binding to the Nicotinic Acetylcholine Receptor

Sébastien Dutertre, Annette Nicke and Richard J. Lewis

J. Biol. Chem. 2005, 280:30460-30468.
doi: 10.1074/jbc.M504229200 originally published online June 1, 2005
